

## THE LIKELY *FERMI* DETECTION OF THE SUPERNOVA REMNANT RCW 103

YI XING<sup>1</sup>, ZHONGXIANG WANG<sup>1</sup>, XIAO ZHANG<sup>2</sup>, & YANG CHEN<sup>2,3</sup>

*Draft version October 31, 2018*

### ABSTRACT

We report on the results from our  $\gamma$ -ray analysis of the supernova remnant (SNR) RCW 103 region. The data were taken with the Large Area Telescope on board the *Fermi Gamma-ray Space Telescope*. An extended source is found at a position consistent with that of RCW 103, and its emission was only detected above 1 GeV ( $10\sigma$  significance), having a power-law spectrum with a photon index of  $2.0 \pm 0.1$ . We obtain its 1–300 GeV spectrum, and the total flux gives a luminosity of  $8.3 \times 10^{33}$  erg s<sup>-1</sup> at a source distance of 3.3 kpc. Given the positional coincidence and property similarities of this source with other SNRs, we identify it as the likely *Fermi*  $\gamma$ -ray counterpart to RCW 103. Including radio measurements of RCW 103, the spectral energy distribution (SED) is modeled by considering emission mechanisms based on both hadronic and leptonic scenarios. We find that models in the two scenarios can reproduce the observed SED, while in the hadronic scenario the existence of SNR–molecular-cloud interaction is suggested as a high density of the target protons is required.

*Subject headings:* acceleration of particles — gamma rays: ISM — ISM: individual objects (RCW 103)  
— ISM: supernova remnants

### 1. INTRODUCTION

The properties of the supernova remnant (SNR) RCW 103 (G332.4-0.4) has been studied at multiple energies, and the SNR is well known as it contains an enigmatic central compact object (CCO; 1E 161348–5055, hereafter 1E 1613). Having a size of  $\sim 10'$  in diameter (Caswell et al. 1980; Tuohy & Garmire 1980), it was determined from optical imaging to have a shell expansion rate of 1100 km s<sup>-1</sup> (Carter et al. 1997) for a source distance of 3.3 kpc (Caswell et al. 1975). This expansion rate implies an age of approximately 2000 yrs. The mid- and near-infrared property characteristic of molecular shock, the nearby H<sub>2</sub> emission, and the HCO<sup>+</sup> morphological feature suggests that it is interacting with a molecular cloud (see Jiang et al. 2010 and references therein). Although it appears similar to typical CCOs by being radio-quiet and not having non-thermal point-source and extended emission (for detailed properties of CCOs, see Pavlov et al. 2004; de Luca 2008; and more recently Gotthelf, Halpern, & Alford 2013), the X-ray point source located in the center of RCW 103 (Tuohy & Garmire 1980) shows strong X-ray variability (Gotthelf et al. 1999) and has an X-ray periodicity of 6.67 hr (De Luca et al. 2006; Esposito et al. 2011), making itself unique among known young neutron stars. The properties of this young neutron star is poorly understood, and different possibilities have been proposed (Li 2007; Pizzolato et al. 2008; Bhadkamkar & Ghosh 2009; Ikhsanov et al. 2013).

SNRs are known to have high-energy non-thermal emission, arising from the shocks of SN explosions. With the great capabilities of the *Fermi Gamma-ray Space*

*Telescope*, many SNRs have been detected at its GeV  $\gamma$ -ray energies. Several of them are known to contain CCOs, and they are Cassiopeia A (Cas A; Abdo et al. 2010c), Vela Jr. (G266.2–1.2; Tanaka et al. 2011), Puppis A (Pup A; Hewitt et al. 2012), and PKS 1209–51/52 (G296.5+10.0; Araya 2013). Similar to other SNRs at the GeV energy range, these young SNRs that harbor a CCO generally have extended power-law emission with photon indices of  $\sim 2$ . With the current *Fermi* measurements, both a leptonic or a hadronic scenario can describe the observed broad-band spectra, while for individual sources one of the scenarios may be slightly more favored (see, e.g., Araya 2013 and references therein). No indication of GeV emission from the CCOs has been found; note that for the CCOs in Pup A and PKS 1209–51/52, their spin periods are known from X-ray timing (Gotthelf et al. 2013 and references therein).

In this paper we present our analyses of the *Fermi* data of the RCW 103 region, and report the likely detection of its GeV emission. In Section 2 the *Fermi* observations are described, and in Section 3 different data analyses and results are given. We discuss our results in Section 4.

### 2. OBSERVATIONS

The Large Area Telescope (LAT) is a  $\gamma$ -ray imaging instrument on board the *Fermi Gamma-ray Space Telescope*, which continuously scans the whole sky every three hours in energy range from 20 MeV to 300 GeV (Atwood et al. 2009). In our analyses we selected LAT events inside a  $20^\circ \times 20^\circ$  region centered at the position of the SNR RCW 103 from the *Fermi* Pass 7 database. The time period of the data is from 2008-08-04 15:43:36 (UTC) to 2013-09-09 00:40:00 (UTC). We rejected events below 200 MeV because of the relative large uncertainties of the instrument response function of the LAT in the low energy range. In addition we only included events with event zenith angles less than 100 degrees to prevent the Earth's limb contamination, and during good time intervals when the quality of the data was not affected by the spacecraft events. These selections are recommended by

<sup>1</sup> Key Laboratory for Research in Galaxies and Cosmology, Shanghai Astronomical Observatory, Chinese Academy of Sciences, 80 Nandan Road, Shanghai 200030, China

<sup>2</sup> Department Astronomy, Nanjing University, 22 Hankou Road, Nanjing 210093, China

<sup>3</sup> Key Laboratory of Modern Astronomy and Astrophysics, Nanjing University, Ministry of Education, Nanjing 210093, China

the LAT team.

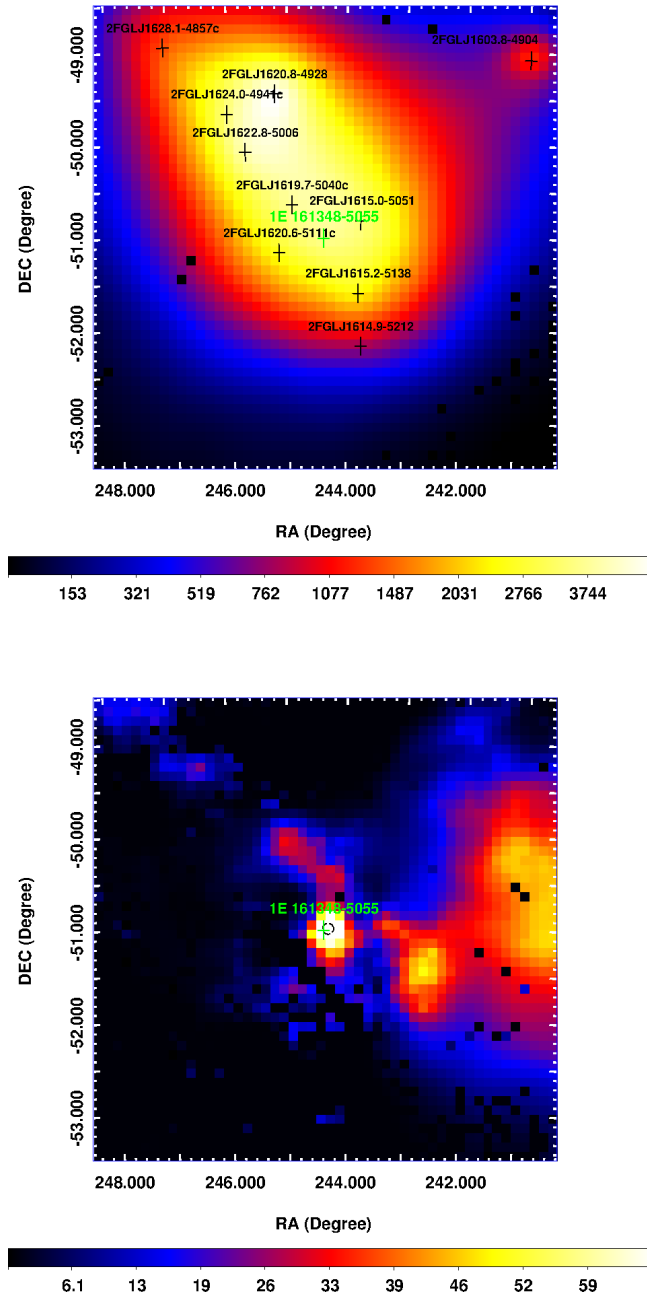


FIG. 1.— 200 MeV–300 GeV TS maps of the  $5^\circ \times 5^\circ$  region centered at RCW 103. The image scales of the maps are  $0.1^\circ \text{ pixel}^{-1}$ . *Upper panel*: sources in the source model outside of the region were considered, with sources in the *Fermi* 2-year catalog within the region marked. *Bottom panel*: all sources in the source model were considered. The dashed circle indicates the  $2\sigma$  error circle of the best-fit position for the residual emission found at the position of RCW 103.

### 3. ANALYSIS AND RESULTS

#### 3.1. Source Identification

We first included all sources within 15 degrees centered at the position of RCW 103 (CCO’s position: R.A.= $16^{\text{h}}17^{\text{m}}36^{\text{s}}.3$ , Decl.= $-51^\circ02'24''.5$ , equinox

J2000.0; Pavlov et al. 2004) in the *Fermi* 2-year catalog (Nolan et al. 2012) to make the source model. The spectral function forms of these sources are provided in the catalog. We let the spectral normalization parameters of the sources within 4 degrees from RCW 103 free, and fixed all the other parameters of the sources to their catalog values. We also included the spectrum model `gal_2yearp7v6_v0.fits` and the spectrum file `iso_p7v6source.txt` in the source model to consider the galactic and the extragalactic diffuse emission, respectively. The parameters ‘Value’ of the Galactic diffuse emission model and ‘Normalization’ of the extragalactic diffuse emission model were let free. We performed standard binned likelihood analysis to the LAT data with the LAT science tools software package `v9r31p1`, and extracted the Test Statistic (TS) map of a  $5^\circ \times 5^\circ$  region centered at the position of RCW 103. A source map considering sources in the source model outside of the region was made, which is shown in the upper panel of Figure 1. It can be seen from the TS map that RCW 103 is located in a very complex region.

After considering and removing all the sources in the source model in this region, we then made a residual map, which is shown in the bottom panel of Figure 1. As can be seen, excess  $\gamma$ -ray emission remained near the center, and  $\text{TS} \simeq 60$ , indicating  $\sim 8\sigma$  detection significance. We ran `gtfindsrc` in the LAT software package to find the best-fit position of the excess  $\gamma$ -ray emission and obtained a position of R.A.= $244^\circ319$ , Decl.= $-51^\circ0261$ , (equinox J2000.0), with  $1\sigma$  nominal uncertainty of  $0^\circ03$ . In addition, detailed analysis indicated that the excess emission only appeared above 1 GeV, as the TS value at the region was nearly zero when only the energy range of 0.2–1 GeV was used. A TS map was thus made with  $\geq 1$  GeV photons from the RCW 103 region and a region of  $1^\circ \times 1^\circ$  centered at RCW 103 is shown Figure 2. The detection significance now is improved to  $\simeq 10\sigma$  ( $\text{TS} > 100$ ). The CCO 1E 1613 centered at RCW 103 is located slightly outside of the  $1\sigma$  error circle with an angular separation of  $0^\circ05$ , but within the  $2\sigma$  error circle.

There are two nearby sources that could be associated with the excess emission, which are PSR J1617–5055 and HESS J1616–508 (Aharonian et al. 2006). Landi et al. (2007) analyzed archival X-ray data and suggested that the HESS source is the pulsar wind nebula (PWN) powered by J1617–5055. In Figure 2, the pulsar’s location and the source size ( $16'$  diameter) of HESS J616–508 are marked. The pulsar is  $\approx 3.7\sigma$  away from our *Fermi* source, and in § 4 we argue that the *Fermi* source is not likely the associated PWN on the basis of spectral property comparison and source positions.

Both PWNe and SNRs are the main sources detected by the HESS survey of the Galactic plane (see, e.g., Carrigan et al. 2013) at its TeV energy range. Lande et al. (2012) searched through sources in the *Fermi* 2-year catalog and found that 2FGL J1615.0–5051 (see the top panel of Figure 1) is extended and spatially coincident with HESS J1616–508, suggesting that they are very likely associated (see also Acero et al. 2013). In our analysis above, 2FGL J1615.0–5051 was treated as a point source, which might not be appropriate if it is truly extended (note that because of source crowdedness, contamination between

the sources can not be avoided). We tested to include 2FGL J1615.0–5051 as an extended source (0.32 deg size; Lande et al. 2012) in the source model, and found that excess emission was still detected at the same position but with  $TS \simeq 40$ . We further checked the fit improvement by calculating the significance values (estimated from  $\sqrt{2 \log(L_2/L_1)}$ , where  $L$  is the likelihood value; e.g., Lande et al. 2012) for different setups of 2FGL J1615.0–5051 and the new *Fermi* source. In the calculation, the model for  $L_1$  only had the extended source given by Lande et al. (2012), and the models for  $L_2$  had 2FGL J1615.0–5051 plus the new *Fermi* source, both being either a point source or an extended source (for the latter case for the new *Fermi* source, a uniform disk with a radius of  $0^\circ.3$  was used; see below § 3.2). We found that the lowest significance value was 5.5 when 2FGL J1615.0–5051 and the new *Fermi* source were the extended source and a point source, respectively, and the highest value was 10.2 when the first and the latter were a point source and an extended source, respectively. The analyses indicate that not only the new *Fermi* source was clearly detected but also a point source 2FGL J1615.0–5051 is more favored.

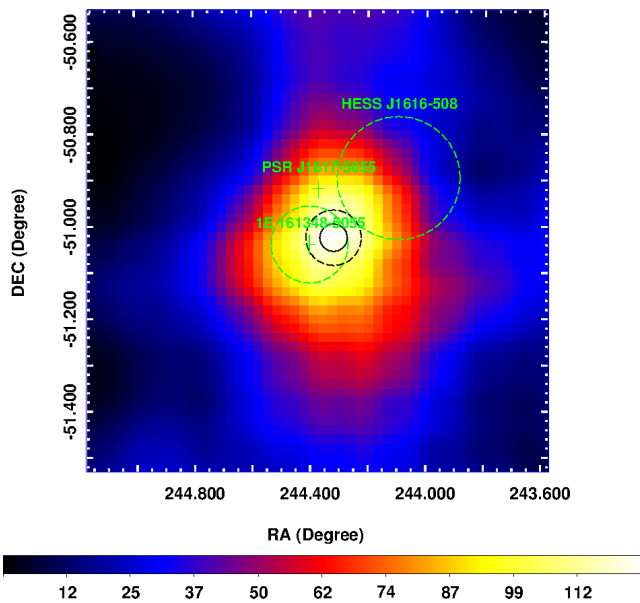


FIG. 2.— Residual 1–300 GeV TS maps of  $1^\circ \times 1^\circ$  region centered at RCW 103. The image scale of the maps is  $0^\circ.02 \text{ pixel}^{-1}$ . The *Fermi* source’s  $1\sigma$  and  $2\sigma$  positional error circles are marked by black solid and dashed circles, respectively, the RCW 103 region centered at the CCO is marked by a green dashed circle, and the positions of PSR J1617–5055 and HESS J1616–508 are also marked, with the latter indicated by the larger green dashed circle.

### 3.2. Spatial Distribution Analysis

We analyzed the spatial distribution of the new *Fermi*  $\gamma$ -ray source at RCW 103 to determine whether the excess emission is point-like or extended. We used both a point source with a power-law spectrum at the best-fit position and uniform disk models with power-law spectra to analyze the emission in the 30–300 GeV range. The searched radius range for the uniform disks was  $0^\circ.1$ – $0^\circ.5$

(see Table 1), and the high energy range was used for the optimal spatial resolution. Additionally in the analysis, only front converting events for the instrument response function P7SOURCE\_V6::FRONT were included, which allows to reduce the point-spread function (PSF) of the LAT to  $<0^\circ.15$  (68% containment). We fixed the power-law indices at 2 for the models (obtained from likelihood analysis in  $>1$  GeV energy range; see below § 3.3) to reduce the uncertainties. For the point source, we let the spectral normalization parameters of the sources within 4 degrees from RCW 103 free, and fixed all the other parameters of the sources in the source model at the *Fermi* 2-year catalog values (2FGL J1615.0–5051 was included as a point source on the basis of our analyses above in § 3.1). For the disk models, we fixed all spectral parameters of the sources in the source model at the values obtained above, but let the spectral normalization parameters of the disk models free. We obtained a TS of 24 for the point source model and a maximum TS value of 37.5 at the radius of  $0^\circ.3$  for the disk models, although we note that the TS values for the radius range of  $0^\circ.16$ – $0^\circ.3$  do not indicate any significant differences (Table 1). Comparing the TS values, our analysis implies  $>3\sigma$  detection of the source extension (the significance was calculated from  $\sqrt{TS_{disk} - TS_{point}}$ ; see, e.g., Lande et al. 2012). The obtained photon fluxes for these models are given in Table 1.

### 3.3. Spectral Analysis

From our likelihood analysis, the excess  $\gamma$ -ray emission was found to be detected only above  $\sim 1$  GeV. Different source models with a power-law spectrum of  $dN/dE = N_0 E^{-\Gamma}$ , which included a point source or extended sources at the best-fit position, were added to the source model, and the emission was found to have  $\Gamma$  of 1.9–2.0 with an uncertainty of 0.1. Given the above results from § 3.1 and § 3.2, we report our  $\gamma$ -ray spectrum result by considering the excess  $\gamma$ -ray emission as an extended source with a size radius of  $0^\circ.3$  at the best-fit position. The  $\gamma$ -ray spectrum was obtained by performing maximum likelihood analysis to the LAT data in 5 evenly divided energy bands in logarithm from 1–300 GeV. Similar to those of the other SNRs, the obtained spectrum has a relative flat energy distribution with a photon index of  $\Gamma = 2.0 \pm 0.1$ . The energy and flux values at the 5 bands are given in Table 2. The total 1–300 GeV luminosity was  $8.3 \times 10^{33} (D/3.3 \text{ kpc})^2 \text{ erg s}^{-1}$ , where source distance  $D = 3.3 \text{ kpc}$  was used for RCW 103 (Caswell et al. 1975).

### 3.4. Timing Analysis

We performed timing analysis to the *Fermi*/LAT data of the RCW 103 CCO region to search for any modulations. The LAT data within  $0^\circ.2$  from the position of the CCO 1E 1613 were folded at its 6.67 hr periodicity (De Luca et al. 2006; Esposito et al. 2011), and two energy ranges, 0.2–300 GeV and 1–300 GeV, were respectively used. No modulations at the period were detected. The values from the  $H$  test (de Jager 1994) obtained from the folded light curves were 0.2 and 0.1 in the ranges of 0.2–300 GeV and 1–300 GeV, respectively, which are significantly small. The value of  $H = 42$  is used by the LAT team to confirm  $\gamma$ -ray pulsations

(Abdo et al. 2010d).

In addition we also constructed 1000 s binned light curves in the above two energy ranges, which were obtained using *Fermi*/LAT aperture photometry analysis. An aperture radius of  $0\text{.}2$  was used. The power spectra in the two energy ranges were extracted. The exposures used to determine the flux in each time bins were calculated assuming a power-law spectrum with  $\Gamma = 2$ . No modulations in the two energy ranges were detected.

We tested to increase the radius used for epoch folding and aperture photometry analysis to  $0\text{.}4$ , but no modulation at the known period or other periods were detected. The obtained  $H$  values for the folded light curves were similarly small (0.5 and 1.9) as those given in the above in the two energy ranges.

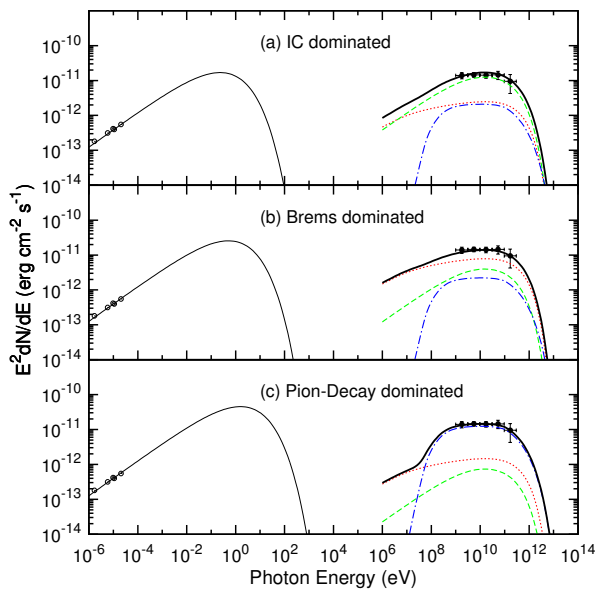


FIG. 3.— *Fermi*  $\gamma$ -ray SED of RCW 103. Radio measurements of the SNR are also included. Three emission components due to IC scattering (green dashed curve), bremsstrahlung (red solid curve), and  $\pi^0$  decay (blue dash-dotted curve) are combined to fit the SED.

#### 4. DISCUSSION

Analyzing the *Fermi*/LAT data of the RCW 103 region, we found an extended  $\gamma$ -ray source with  $\sim 10\sigma$  significance at a position consistent with that of the young SNR. It should be cautiously noted that as shown in both Figures 1 and 2, the source is located in a complex region. A few known *Fermi*  $\gamma$ -ray sources, the young pulsar J1617–5055, and HESS J1616–508 are nearby. The intensity-peak position of this *Fermi* source also appears to have a  $\sim 0\text{.}05$  offset from the center of RCW 103 (however the intensity peak position roughly coincides with the north-west edge of the X-ray shell which overlaps one bright  $H_2$  region; see Oliva et al. 1990). We determined that the *Fermi* source probably had a radius of as small as  $\sim 0\text{.}16$ , which is approximately double the size of the SNR seen at X-ray and radio energies. However

the property similarity of the source and the other SNRs strongly supports the detection of *Fermi*  $\gamma$ -ray emission from RCW 103. For example for those young SNRs harboring a CCO, they all have prominent emission at energies above 1 GeV, and the spectra are a power law with photon indices in a range of 1.85–2.1, which makes their spectral energy distributions (SEDs) flat in the energy range. At similar distances, they have luminosities of  $10^{33}$ – $10^{34}$  erg  $s^{-1}$ . The detection of  $H_2$  lines in the region right outside of the remnant shell of RCW 103 suggests that the remnant is interacting, probably fractionally, with a molecular cloud (Oliva et al. 1990; see also Jiang et al. 2010). The ‘normal’  $\gamma$ -ray luminosity value we derived for RCW 103 is consistent with the picture, as the SNRs that are known to be interacting with molecular clouds have luminosities at least one order of magnitude higher because of the high target masses of molecular clouds (e.g., Abdo et al. 2009; Castro & Slane 2010).

The pulsar J1617–5055 (having a spin-down age of 8.1 kyr; Torii et al. 1998; Kaspi et al. 1998) is located  $3.7\sigma$  away from the position of the detected *Fermi* source. Since electrons responsible for  $\gamma$ -ray emission of PWNe via inverse Compton (IC) scattering are thought to be ‘old’ (i.e., they are less energetic and have longer lifetimes than those X-ray emitting electrons detected around pulsars due to synchrotron radiation; e.g., Mattana et al. 2009; de Jager et al. 2009), a significant offset between a fast-moving pulsar and its GeV/TeV PWN might appear (e.g., Kargaltsev et al. 2013). However, the currently confirmed *Fermi* PWNe all have harder power-law spectra with photon indices in a range of 1.4–1.6 (e.g., the Crab pulsar, Abdo et al. 2010b; PSR B1509–58, Abdo et al. 2010a; PSR J1838–0655, Lande et al. 2012; PSR J1856+0245, Rousseau et al. 2012; PSR B1823–13, Grondin et al. 2011), making their SEDs clearly rising in the *Fermi* energy range. The difference in the spectral properties of these PWNe and the SNRs is distinguishable. Moreover, even if the  $\gamma$ -ray source is a PWN powered by J1617–5055, it would imply that the pulsar not only moved away from a sky region coinciding with RCW 103, raising the issue again about whether or not they are associated (Kaspi et al. 1998), but also has to have an extremely large transverse velocity ( $\sim 4200$  km  $s^{-1}$ ; see Kaspi et al. 1998 for detailed discussion). The current studies of RCW 103 and the pulsar do not support either of them.

We searched in the SIMBAD Astronomical Database within the  $2\sigma$  error circle of the best-fit position of the  $\gamma$ -ray source, but only a few normal stars besides RCW 103 and its CCO are known in the region. Given all these, we conclude that *Fermi*  $\gamma$ -ray emission from the SNR RCW 103 was likely detected, although contamination from nearby  $\gamma$ -ray sources due to the low spatial resolution of the LAT is possible (Figure 1; a TS of  $\sim 2000$  at the position of RCW 103 when the nearby sources are kept versus a TS of  $\sim 60$  in the residual map).

With the conclusion, we studied the SED of RCW 103 by considering both the hadronic and leptonic scenarios. In the scenarios, a power-law spectrum with a cut-off energy  $E_{i,cut}$  for particles of electrons and protons is assumed:

$$dN_i/dE_i = A_i E_i^{-\alpha_i} \exp(-E_i/E_{i,cut}), \quad (1)$$

where  $i = e, p$ ,  $E_i$  is the particle kinetic energy,  $\alpha_i$  is the spectral index, and  $A_i$  is the normalization factor. A ratio of  $K_{ep} = A_e/A_p$  compares the number of the electrons to that of the protons at a given energy. We included the radio flux measurements of the SNR (Beard 1966; Goss & Shaver 1970; Shaver & Goss 1970; Caswell et al. 1980; Dickel et al. 1996) as additional constraints, which can be described by a power law with a spectral index of  $-0.56$  (Figure 3; Dickel et al. 1996). In the hadronic scenario,  $\gamma$ -rays are emitted due to the decay of  $\pi^0$  mesons produced in collisions of the protons with ambient gas, and in the leptonic scenario, IC scattering or bremsstrahlung emission by/from high-energy electrons contributes dominantly to the observed  $\gamma$ -rays. We refer to Zhang et al. (2013) and references therein for calculation details.

We found that both scenarios can describe the SED. Our model spectra that are dominated by IC scattering, bremsstrahlung, or  $\pi^0$  decay components are shown in the upper, middle, and bottom panel of Figure 3, respectively. In the calculations, an energy density of  $0.5 \text{ eV cm}^{-3}$  for the interstellar radiation field at the location (Porter et al. 2006) was used,  $\alpha_e = 2.0$  was needed to fit the radio data points, and  $\alpha_p = 2.0$ ,  $E_{e,cut} = 1 \text{ TeV}$ , and  $E_{p,cut} = 3 \text{ TeV}$  were found to be able to provide a good fit to the  $\gamma$ -ray part. Our model fluxes at the X-ray energy range of  $0.2\text{--}10 \text{ keV}$  is generally below  $10^{-14} \text{ erg cm}^{-2} \text{ s}^{-1}$ , which may explain the non-detection of a power-law component in the X-ray spectrum of the SNR (Nugent et al. 1984; Gotthelf et al. 1997). The X-ray emission from the SNR is well described by a non-equilibrium ionization (NEI) plasma model at temperature  $0.3 \text{ keV}$  with a large (unabsorbed) flux of  $\sim 10^{-9} \text{ erg cm}^{-2} \text{ s}^{-1}$  (estimated from the *Einstein Observatory* detection; Seward 1990). The values required for other parameters in our calculations, including  $K_{ep}$ , the magnetic field strength  $B$ , the average density of the target baryons (with which the energetic particles interact)  $n_t$ , the total energy of protons  $W_p$ , and the total energy of electrons  $W_e$ , are summarized in Table 3. In the  $\pi^0$  decay model,  $W_p = 0.75 \times 10^{50} (n_t/10 \text{ cm}^{-3})^{-1}$  was needed. If we constrain  $W_p$  to be smaller than 50% of  $E_0$ , where  $E_0$  is the total blast energy, we have  $n_t > 1(E_0/10^{51} \text{ erg})^{-1} \text{ cm}^{-3}$ . From the X-ray spectral analysis of the SNR with the NEI plasma model, the density of the X-ray emitting gas  $n_x$  was estimated to be  $n_x \approx 0.3 \pm 0.1 (E_0/10^{51} \text{ erg})^{-1/2} \text{ cm}^{-3}$  (Nugent et al. 1984; see also Gotthelf et al. 1997). In the hadronic scenario in which the relativistic protons impact the adja-

cent molecular clouds, such a low  $n_x$  value does not contradict the above large  $n_t$  estimate. This is because the  $n_t$  value includes the contribution of the baryons in the dense molecular clumps, while  $n_x$  reflects the low density of the interclump hot gas. Therefore, the hadronic model seems to be consistent with the context of shock-molecular-cloud interaction.

Based on the current *Fermi* measurements, the cut-off energies for electrons and protons in our models are at  $\sim 1 \text{ TeV}$ . Thus far no very high energy (VHE) TeV detection of a source at the position of RCW 103 has been reported (e.g., Carrigan et al. 2013). If HESS J1616–508 is the associated TeV nebula, in addition to the apparent positional offset, its flux at  $\sim 200 \text{ GeV}$  (Aharonian et al. 2006) would also be slightly larger (by a factor of  $\sim 2$ ) than the *Fermi* value we obtained. Comparing to other CCO SNRs with ages of several thousands years, while the SED of Vela Jr. has a prominent TeV component (Aharonian et al. 2007) and starts decreasing from above  $\sim 1 \text{ TeV}$ , resulting  $>10 \text{ TeV}$  cut-off energies (Tanaka et al. 2011), the SEDs of RCW 103 and Pup A (Hewitt et al. 2012) are rather similar, as they both start decreasing above  $10 \text{ GeV}$  and thus are modeled to have low cut-off energies at  $\sim 1 \text{ TeV}$  (PKS 1209–51/52 is not included in discussion here since it was weakly detected by *Fermi*; Araya 2013). The fact that both RCW 103 and Pup A are in the vicinity of molecular clouds (e.g., Hewitt et al. 2012) could be the reason for the similar low cut-off energies, as particles from SN explosion shocks is possibly limited to have relatively low energies due to the interaction with high-density ambient gas (e.g., Sturmer et al. 1997). The detectability of Pup A by the current generation Cherenkov telescopes has been pointed out by Hewitt et al. (2012), particularly since it is not located in a complex region and has a relatively high Galactic latitude of  $-3^\circ.4$ . We note that based on our current models, the TeV counterpart to RCW 103 should be detectable, as the HESS survey of the Galactic plane had a sensitivity limit of  $\sim 10^{-12} \text{ erg cm}^{-2} \text{ s}^{-1}$  at  $1 \text{ TeV}$  (Aharonian et al. 2006), lower than our model fluxes at the energy.

We thank P. H. T. Tam for help with understanding the HESS survey of the Galactic plane and the sensitivity.

This research was supported by National Natural Science Foundation of China (11073042, 11373055, and 11233001). ZW is a Research Fellow of the One-Hundred-Talents project of Chinese Academy of Sciences.

## REFERENCES

- Abdo, A. A., Ackermann, M., Ajello, M., et al. 2009, *ApJ*, 706, L1  
 —. 2010a, *ApJ*, 714, 927  
 —. 2010b, *ApJ*, 708, 1254  
 —. 2010c, *ApJ*, 710, L92  
 Abdo, A. A., et al. 2010d, *ApJS*, 187, 460  
 Acero, F., et al. 2013, *ApJ*, 773, 77  
 Aharonian, F., Akhperjanian, A. G., Bazer-Bachi, A. R., et al.  
 2006, *ApJ*, 636, 777  
 —. 2007, *ApJ*, 661, 236  
 Araya, M. 2013, *MNRAS*, 434, 2202  
 Atwood, W. B., et al. 2009, *ApJ*, 697, 1071  
 Beard, M. 1966, *Australian Journal of Physics*, 19, 141  
 Bhadkamkar, H., & Ghosh, P. 2009, *A&A*, 506, 1297  
 Carrigan, S., Brun, F., Chaves, R. C. G., Deil, C., Gast, H.,  
 Marandon, V., & for the H. E. S. S. collaboration. 2013, *ArXiv e-prints*  
 Carter, L. M., Dickel, J. R., & Bomans, D. J. 1997, *PASP*, 109,  
 990  
 Castro, D., & Slane, P. 2010, *ApJ*, 717, 372  
 Caswell, J. L., Haynes, R. F., Milne, D. K., & Wellington, K. J.  
 1980, *MNRAS*, 190, 881  
 Caswell, J. L., Murray, J. D., Roger, R. S., Cole, D. J., & Cooke,  
 D. J. 1975, *A&A*, 45, 239  
 de Jager, O. C. 1994, *ApJ*, 436, 239  
 de Jager, O. C., et al. 2009, *ArXiv e-prints*

TABLE 1  
SPATIAL DISTRIBUTION ANALYSIS RESULTS FOR THE EXCESS EMISSION AT RCW 103

Source model	Radius	Flux <sup>a</sup>	TS
Point source	...	2.1±0.7	23.5
Uniform disk	0°1	2.9±0.8	30.3
	0°16	3.5±0.9	36.0
	0°2	3.7±0.9	37.0
	0°3	4.3±1.0	37.5
	0°4	4.8±1.1	33.1
	0°5	5.1±1.2	28.4

NOTE. — The analysis was made in the energy range of 30–300 GeV.

<sup>a</sup> Flux is in units of  $10^{-10}$  photon  $\text{cm}^{-2}$   $\text{s}^{-1}$ .

TABLE 2  
*Fermi*/LAT SPECTRAL DATA POINTS

$E$ (GeV)	$E^2 dN(E)/dE$ ( $10^{-11}$ erg $\text{cm}^{-2}$ $\text{s}^{-1}$ )	TS
1.8	1.67±0.34	55.8
5.5	1.76±0.26	71.2
17.3	1.71±0.31	49.7
54.2	1.74±0.46	27.1
169.6	1.14±0.63	6.6

TABLE 3  
PARAMETERS FOR THE HADRONIC AND LEPTONIC MODELS

Model	$K_{ep}$	$B$ ( $\mu\text{G}$ )	$n_t$ ( $\text{cm}^{-3}$ )	$W_p$ (erg)	$W_e$ (erg)
IC	0.1	5.5	1	$1.3 \times 10^{50}$	$1.1 \times 10^{49}$
Brem.	0.3	12	10	$1.4 \times 10^{49}$	$0.35 \times 10^{49}$
$\pi^0$ decay	0.01	35	10	$7.5 \times 10^{49}$	$0.065 \times 10^{49}$

NOTE. —  $\alpha_e = 2.0$ ,  $E_{e,cut} = 1$  TeV,  $\alpha_p = 2.0$ , and  $E_{p,cut} = 3$  TeV were used for all the models. The energy density for the interstellar radiation field at the location was  $0.5$  eV  $\text{cm}^{-3}$  (Porter, Moskalenko, & Strong 2006).

- de Luca, A. 2008, in American Institute of Physics Conference Series, Vol. 983, 40 Years of Pulsars: Millisecond Pulsars, Magnetars and More, ed. C. Bassa, Z. Wang, A. Cumming, & V. M. Kaspi, 311–319
- De Luca, A., Caraveo, P. A., Mereghetti, S., Tiengo, A., & Bignami, G. F. 2006, *Science*, 313, 814
- Dickel, J. R., Green, A., Ye, T., & Milne, D. K. 1996, *AJ*, 111, 340
- Esposito, P., Turolla, R., de Luca, A., Israel, G. L., Possenti, A., & Burrows, D. N. 2011, *MNRAS*, 418, 170
- Goss, W. M., & Shaver, P. A. 1970, *Australian Journal of Physics Astrophysical Supplement*, 14, 1
- Gotthelf, E. V., Halpern, J. P., & Alford, J. 2013, *ApJ*, 765, 58
- Gotthelf, E. V., Petre, R., & Hwang, U. 1997, *ApJ*, 487, L175
- Gotthelf, E. V., Petre, R., & Vasisht, G. 1999, *ApJ*, 514, L107
- Grondin, M.-H., Funk, S., Lemoine-Goumard, M., et al. 2011, *ApJ*, 738, 42
- Hewitt, J. W., Grondin, M.-H., Lemoine-Goumard, M., Reposeur, T., Ballet, J., & Tanaka, T. 2012, *ApJ*, 759, 89
- Ikhsanov, N. R., Kim, V. Y., Beskrovnaya, N. G., & Pustil'nik, L. A. 2013, *Ap&SS*, 346, 105
- Jiang, B., Chen, Y., Wang, J., Su, Y., Zhou, X., Safi-Harb, S., & DeLaney, T. 2010, *ApJ*, 712, 1147
- Kargaltsev, O., Rangelov, B., & Pavlov, G. G. 2013, *ArXiv e-prints*
- Kaspi, V. M., Crawford, F., Manchester, R. N., Lyne, A. G., Camilo, F., D'Amico, N., & Gaensler, B. M. 1998, *ApJ*, 503, L161
- Lande, J., Ackermann, M., Allafort, A., et al. 2012, *ApJ*, 756, 5
- Landi, R., de Rosa, A., Dean, A. J., Bassani, L., Ubertini, P., & Bird, A. J. 2007, *MNRAS*, 380, 926
- Li, X.-D. 2007, *ApJ*, 666, L81
- Mattana, F., et al. 2009, *ApJ*, 694, 12
- Nolan, P. L., et al. 2012, *ApJS*, 199, 31
- Nugent, J. J., Pravdo, S. H., Garmire, G. P., Becker, R. H., Tuohy, I. R., & Winkler, P. F. 1984, *ApJ*, 284, 612
- Oliva, E., Moorwood, A. F. M., & Danziger, I. J. 1990, *A&A*, 240, 453
- Pavlov, G. G., Sanwal, D., & Teter, M. A. 2004, in *IAU Symposium*, Vol. 218, Young Neutron Stars and Their Environments, ed. F. Camilo & B. M. Gaensler, 239
- Pizzolato, F., Colpi, M., De Luca, A., Mereghetti, S., & Tiengo, A. 2008, *ApJ*, 681, 530
- Porter, T. A., Moskalenko, I. V., & Strong, A. W. 2006, *ApJ*, 648, L29
- Rousseau, R., Grondin, M.-H., Van Etten, A., et al. 2012, *A&A*, 544, A3
- Seward, F. D. 1990, *ApJS*, 73, 781
- Shaver, P. A., & Goss, W. M. 1970, *Australian Journal of Physics Astrophysical Supplement*, 14, 77
- Sturmer, S. J., Skibo, J. G., Dermer, C. D., & Mattox, J. R. 1997, *ApJ*, 490, 619
- Tanaka, T., et al. 2011, *ApJ*, 740, L51
- Torii, K., et al. 1998, *ApJ*, 494, L207
- Tuohy, I., & Garmire, G. 1980, *ApJ*, 239, L107
- Zhang, X., Chen, Y., Li, H., & Zhou, X. 2013, *MNRAS*, 429, L25